Ultrasonics 52 (2012) 333–342

Contents lists available at SciVerse ScienceDirect

Ultrasonics

journal homepage: www.elsevier.com/locate/ultras

Modified synthetic transmit aperture algorithm for ultrasound imaging

Y. Tasinkevych [a,*], I. Trots [a], A. Nowicki [a], P.A. Lewin [a,b]

[a] Institute of Fundamental Technological Research of the Polish Academy of Sciences, Pawinskiego 5B, Warsaw 02-106, Poland
[b] Drexel University, Philadelphia, PA 19104, USA

ARTICLE INFO

Article history:
Received 24 August 2011
Received in revised form 6 September 2011
Accepted 7 September 2011
Available online 22 September 2011

Keywords:
Synthetic aperture imaging
Ultrasound imaging
Directivity function
Beamforming

ABSTRACT

The modified synthetic transmit aperture (STA) algorithm is described. The primary goal of this work was to assess the possibility to improve the image quality achievable using synthetic aperture (SA) approach and to evaluate the performance and the clinical applicability of the modified algorithm using phantoms. The modified algorithm is based on the coherent summation of back-scattered RF echo signals with weights calculated for each point in the image and for all possible combinations of the transmit–receive pairs. The weights are calculated using the angular directivity functions of the transmit–receive elements, which are approximated by a far-field radiation pattern of a narrow strip transducer element vibrating with uniform pressure amplitude over its width. In this way, the algorithm takes into account the finite aperture of each individual element in the imaging transducer array. The performance of the approach developed was tested using FIELD II simulated synthetic aperture data of the point reflectors, which allowed the visualization (penetration) depth and lateral resolution to be estimated. Also, both simulated and measured data of cyst phantom were used for qualitative assessment of the imaging contrast improvement. The experimental data were obtained using 128 elements, 4 MHz, linear transducer array of the Ultrasonix research platform. The comparison of the results obtained using the modified and conventional (unweighted) STA algorithms revealed that the modified STA exhibited an increase in the penetration depth accompanied by a minor, yet discernible upon the closer examination, degradation in lateral resolution, mainly in the proximity of the transducer aperture. Overall, however, a considerable (12 dB) improvement in the image quality, particularly in the immediate vicinity of the transducer's surface was demonstrated. The modified STA method holds promise to be of clinical importance, especially in the applications where the quality of the "near-field" image, that is the image in the immediate vicinity of the scanhead is of critical importance such as for instance in skin- and breast-examinations.

1. Introduction

In the past decade ultrasound imaging has become one of the preferred diagnostic techniques primarily because of its accessibility, the use of non-ionizing radiation, and real-time display. High resolution (defined later in terms of the wavelength) ultrasound images are routinely obtained by employing phased array transducers and delay-and-sum beamforming techniques. In this approach, however, the adequate focusing of the examined volume is achieved at the expense of the limited frame rate. Often, this time frame is reduced to below 15 fps, which in practice means that the image cannot be produced in real time [1,2].

The primary goal of this work was to assess the possibility to improve the image quality achievable using synthetic aperture (SA) approach and to evaluate the performance and the clinical applicability of the modified algorithm using phantoms.

Although several [3–5] different implementations of SA method of this technique were reported, the synthetic transmit aperture (STA) technique described in Ref. [6] is most directly relevant to the deliberations presented below. It uses all elements of the imaging transducer in receive mode at each transmission and ensures the full dynamic focusing in both transmit and receive modes, which provides the imaging quality comparable to that achievable with the conventional phased arrays.

The brief discussion that follows indicates that whereas the modified STA proposed here is not capable of providing 1000 frames per second (fps) display achievable with coherent plane-wave compounding [2], a feature of recently commercially introduced supersonic imaging (SSI) [7], it is capable of delivering images on the order of 100 fps. Such rate is still approximately four times faster than the frame rate of conventional imaging equipment and hence seem to support the notion that the image optimization method described in this work is warranted. Further – as evidenced below – the resulting enhanced image resolution holds promise to augment the diagnostic power of ultrasound modality in the skilled physician's hands.

* Corresponding author.
E-mail address: yurijtas@ippt.gov.pl (Y. Tasinkevych).

0041-624X/$ - see front matter © 2011 Elsevier B.V. All rights reserved.
doi:10.1016/j.ultras.2011.09.003

It is well known that the conventional line scanning technique employed in currently used ultrasound scanners suffers from the trade-off between the number of focusing zones and the frame rate. The reduction in the frame rate is proportional to the number of foci introduced to optimize the lateral (most critical) resolution of the image.

As described in the following, the STA algorithm minimizes the influence of this trade-off deficiency when compared to the coherent plane-wave compounding [2]. The compounding technique assures a very fast (up to 1000 fps) imaging by employing several emissions of unfocused plane-wave probing signals. As mentioned above, this technique is implemented in the SuperSonic Imagine system used for transient elastography [7]. In transient elastography application the highest possible frame rates are required. The considered frame rate of approximately 1000/s can be achieved by the coherent plane-wave compounding using 12 emissions.

It may be useful to note here that the coherent plane-wave compounding would require 45 probing waves yielding about 270 fps to produce image quality (defined in terms of contrast resolution) comparable with the one achievable with the conventional 25 fps, 128 elements array operating with 4 foci and covering penetration depth of 6 cm. In comparison, for the above listed conditions 128 elements array employing STA approach would provide imaging rate in excess of 100/s. This rate could be increased by minimizing the number of probing waves and can be conveniently implemented by making use of the sparse array design [8] and transmission with a section or group of individual elements [8].

In early applications of the STA ultrasound techniques only stationary or still structures could be visualized. This is because the image was constructed based on coherent summation of echo signals acquired from multiple firings by the sub-sets or sub-groups of individual elements as discussed in the next section.

Hence, in contrast to phased array beam formers, the early STA systems were sensitive to motion artefacts; the elegant solution to this problem was devised by the Danish research team [9]. Their extension of the STA technique allowed blood flow imaging and artifact free visualization of anatomic structures such as moving tissue [10].

However, the extension described in Refs. [9–11] considers a single element of a multi-element imaging probe as a point source transmitting a spherical wavefront [11]. This approach is reasonable for elements having their size much smaller than the wavelength of the probing or interrogating signal. Yet, when the element size is comparable to the wavelength of the interrogating wave the influence of the element's directivity on the wave field generation and reception can no longer be neglected. Therefore, an application of the simple point source model to reconstruct the image might lead to errors and artifacts worsening the quality of the overall image.

To address this problem the modified STA method is presented below. The method takes into account the single element directivity when the element's lateral width is comparable with the operating frequency wavelength This is introduced by applying predefined apodization weights evaluated for every focal point in the image in both transmit and receive modes. To this end the analytic expression derived in Ref. [12] for a far-field radiation pattern of a strip geometry (i.e. the geometry where the length of the array element is much longer than its width) transducer is employed. The expression, which is valid for a strip source exhibiting uniform pressure amplitude across its width allows apodization weights to be calculated.

Modification and control of the beam patterns by applying the aperture apodization in the ultrasonic imaging systems was reported in several works [13–15]. Frequently, fixed weights corresponding to Hamming-, Hann-, and Blackman window functions [16,17] are applied to echo signals recorded from different channels during dynamic focusing of the received beam. In addition, in the STA analysis often the transmitted pulse waveform, which influences the contrast resolution needs to be accounted for. To obtain a more flexible control over transmitted and received wave-fields, the specific, optimal sets of weights generated for each focus point in the image are determined. This enables synthetization of the desirable beam patterns [18]. The sets can also be used to obtain the required field distribution at a given, user controlled, depth [19].

As evidenced in the following, in this work the application of proposed apodization weights considerably improves the penetration depth and diminishes the hazy, blurring artefacts observable in the case of the conventional STA algorithm. This improvement in imaging quality is particularly visible in the immediate vicinity (near-field distance) of the transducer surface, which is critical in such applications as breast and skin imaging. To the best of the authors' knowledge the image optimization in the immediate vicinity of the scanhead surface using the STA approach with individual weighting functions was not explored previously.

The paper is organized in the following way. In the next section the brief discussion of the STA algorithm is given.

In Section 3 the modified algorithm is introduced and discussed in details. Numerical examples presenting the performance of the proposed algorithm are shown for 4 MHz 64-element transducer array with 0.3 mm pitch and 0.02 mm kerf using synthetic aperture (SA) data for point reflectors simulated by FIELD II [20,21]. In Section 4 a brief discussion of the experimental setup is given. Also, a 2D visualization of cyst phantom (Dansk Fantom Service, model 571) is shown for measurement data collected using the SonixTOUCH Research system (Ultrasonix Medical Corporation, Richmond, BC, Canada). The comparison between the image produced using the conventional STA, Hamming and Blackman windows enhanced STA and the modified STA algorithms is also presented. Finally, in Section 5 the results of numerical simulations are compared with those obtained experimentally, and in Section 6 the conclusion of this work are summarized.

2. Synthetic transmit aperture algorithm

In this section the principle of the STA algorithm is discussed in a qualitative way; quantified data are presented in Sections 4 and 5. As mentioned earlier synthetic transmit aperture (STA) method [6,8,9] allows full dynamic focusing both in transmit and receive modes yielding high quality of the resulting images, comparable to those obtainable with the conventional phased arrays In the STA approach, a full aperture is synthesized by processing the echoes received from multiple firings. At each firing, all array elements receive back-scattered echoes independently, which are then digitized and stored in memory for further processing. To create a synthesized high resolution image the focusing at each point is performed using the delay-and-sum approach. The corresponding time delays are evaluated based on geometric distances from the transmitting element to the imaging point and back to the receiving element. The structure of the synthetic aperture and geometric relation between the transmit and receive element combination can be conveniently discussed with reference to Fig. 1.

When a short pulse is transmitted by the mth element and the echo signal is received by the nth element, as shown in Fig. 1, the round-trip delay is

$$\tau_{m,n} = \tau_m + \tau_n, \tag{1}$$

where (m,n) is the transmit–receive element combination, $1 \leqslant m, n \leqslant N$. The corresponding delays for mth and nth elements relative to the focus point (r,θ) can be determined from the following equation:

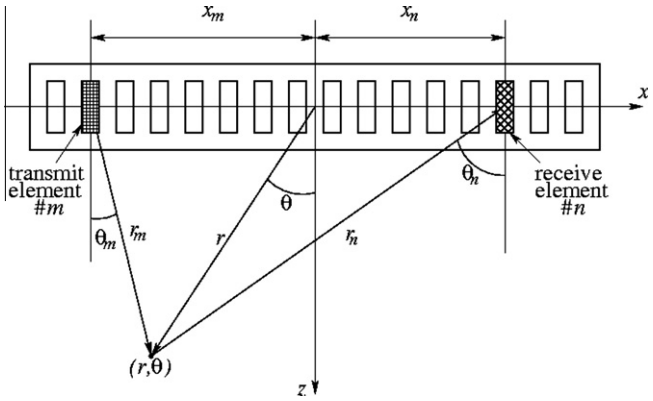

Fig. 1. Geometric relation between the transmit and receive elements combination and the location of the focus.

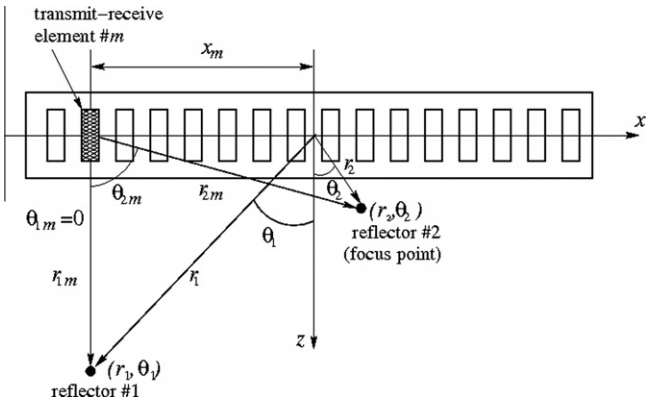

Fig. 2. Influence of the reflector #1 located at the point (r_1,θ_1) on the value of resulting signal $A(r_2,\theta_2)$ for focus point (r_2,θ_2), coinciding with location of reflector #2.

$$\tau_i = \frac{1}{c}\left(r - \sqrt{r^2 + x_i^2 - 2x_i \sin\theta}\right), \quad i = m, n, \tag{2}$$

where x_m, x_n are the positions of the mth transmit and nth receive elements, respectively, and (r,θ) are the polar coordinates of the focus point with respect to the origin located at the center of the transducer's aperture. In the case of the N-element array for each point in the image, the eventually focused signal can be expressed as follows

$$A(r,\theta) = \sum_{m=1}^{N}\sum_{n=1}^{N} y_{m,n}\left(\frac{2r}{c} - \tau_{m,n}\right), \tag{3}$$

where $y_{m,n}(t)$ is the echo signal and $\tau_{m,n}$ is the round-trip delay defined in Eq. (1) for the (m,n) transmit–receive element combination. The first and the second summations correspond to the focusing on transmit and receive, respectively. It should be noted that in this point-like source model the angular dependence is not taken into account. However, as indicated earlier, when the width of the array element is comparable to the working frequency wavelength the point-like source model becomes inadequate. The individual element's directivity pattern influences the partial contributions of the resulting signal $A(r,\theta)$ in Eq. (3). These contributions depend on the mutual positions of the imaging point and transmit–receive pair, determined by the angles θ_m, θ_n (see Fig. 1).

The next section highlights the differences between the STA and the modified STA algorithm developed in the course of this research. Again, the differences are explained in qualitative terms, whereas the quantified data are presented in Sections 4 and 5.

3. Modified synthetic transmit aperture algorithm

In this section a modified STA imaging algorithm which accounts for the element directivity function and its influence on the total signal $A(r,\theta)$ is presented. The underlying idea can be conveniently examined by considering two similar reflectors that are located at the points with polar coordinates (r_i,θ_i); $i = 1, 2$, and introducing the mth element of the transducer array, which acts as transmitter (see Fig. 2). The corresponding RF echo signal received by this element is denoted as $y_{m,m}(t)$. As $r_{1m} = r_{2m}$, both reflectors contribute to the corresponding echo signal $y_{m,m}(t)$ simultaneously due to the equal round-trip propagation time; $2r_{im} = c$; $i = 1, 2$. The scattering amplitude of the reflector #1 located at the point (r_1,θ_1) is dominant, since the angle θ_{1m} coincides with the mth element's normal direction (direction of its maximum radiation), whereas the reflector's transmit–receive efficiency at the angle θ_{2m}, corresponding to the reflector #2, is lower. If the focus point coincides with the location of the reflector #2, the partial contribution from $y_{m,m}(t)$ to $A(r_2,\theta_2)$ evaluated from Eq. (3) introduces the spurious echo from the reflector #1. This is in addition to the signal scattered from the reflector #2 (which is relatively small due to the large observation angle θ_{2m}). Due to its location (the normal direction with respect to the considered mth element), the corresponding false contribution is relatively large, which results in an excessive signal amplitude increase at the point (r_2,θ_2) of the final image. In other words, the scattered signals from distant reflectors (scatterers) are spuriously "transferred" into the region adjacent to the transducer aperture, where the large observation angles exist, and produce an image distortion there. To alleviate this problem, a proper spatial filtering, accounting for the observation angle in accordance with the array element directivity function, is needed. This spatial filtering is implemented by assuming that the angular directivity function of a single element is known and denoted by $f(\theta_m)$, where θ_m is measured from the mth element normal direction (see Fig. 2). To suppress the influence from the reflector #1 on the imaging signal $A(r_2,\theta_2)$ at the focus point (r_2,θ_2), coinciding with location of the reflector #2, the partial contribution of the echo $y_{m,m}(t)$ is weighted by the corresponding value of $f(\theta_{2m})$.

This corresponds to the spatial filtering of the superposed signal in accordance with the positions of the focus point and transmit–receive elements, while accounting for their angular directivity functions. The above considerations lead to the following modification (Eq. (4)) of the STA imaging algorithm

$$A(r,\theta) = \sum_{m=1}^{N}\sum_{n=1}^{N} w_{m,n}(r,\theta) y_{m,n}\left(\frac{2r}{c} - \tau_{m,n}\right),$$
$$w_{m,n}(r,\theta) = f(\theta_m) f(\theta_n), \theta_i = \theta_i(r,\theta), i = m, n, \tag{4}$$

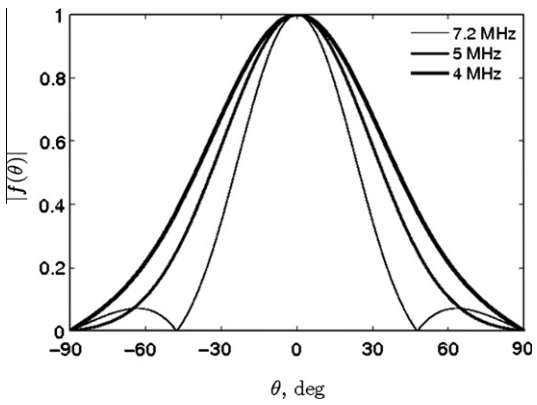

Fig. 3. Directivity functions for transducer array element with $d = 0.28$ mm for different frequencies 4, 5, 7.2 MHz corresponding to $d/\lambda = 0.75, 0.94, 1.35$.

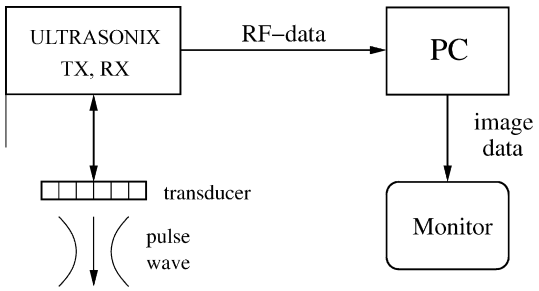

Fig. 4. Block diagram of an ultrasound imaging system. IMPROVE: Mark working frequency – 4 MHz of the transducer, add Matlab info to the PC box.

where $\theta_i(r,\theta)$, $i = m, n$, is the observation angle for the transmit–receive elements. In the proposed modified STA algorithm, Eq. (4), the weights $f(\theta_m)$ for transmit and $f(\theta_n)$ for receive modes are introduced, respectively along with the angles depending on the spatial position of the focal point (r,θ). The directivity function $f(\theta)$, which is used for evaluation of weights $w_{m,n}$, can be calculated using far-field approximation for a single element of the array transducer [12]:

$$f(\theta) = \frac{\sin(\pi d/\lambda \sin\theta)}{\pi d/\lambda \sin\theta}\cos\theta, \tag{5}$$

where d is the element width, and λ is the wavelength. Eq. (5) describes pressure amplitude distribution generated by a strip transducer vibrating with a uniform displacement amplitude along its width. A few representative examples of the directivity patterns determined for a single transducer element having width of $d = 0.28$ mm, and operating at frequencies of 4, 5, and 7.2 MHz are shown in Fig. 3. These patterns correspond to the ratios $d/\lambda = 0.75$, 0.94 and 1.35, respectively and were used in the numerical simulations presented in Section 5.

The patterns shown in Fig. 3 are in agreement with the experimental results reported in Ref. [12] and obey Rayleigh–Sommerfeld formula [22]. It should be noted, that the same function $f(\theta)$ is used both in the transmit and receive modes for evaluation of weights in Eq. (4). The value of λ in Eq. (5) corresponds to the working frequency of the probing wave. The far-field approximation is justified here; for example at the nominal frequency of 4 MHz and the transducer element width of $d = 0.28$ mm, corresponding to the ratio of $d/\lambda = 0.75$ a far-field transition distance can be estimated by utilizing the expression $r_{\min} \approx 2d^2/\lambda$ [23]. The evaluated distance is approximately $1.5\lambda \approx 0.6$ mm and the numerical examples considered in Section 5 used the above values as the simulation input parameters.

4. Methods

A simplified block diagram of the experimental setup used is this work is shown in Fig. 4.

The setup makes use of an Ultrasonix – SonixTOUCH Research System (Ultrasonix Medical Corporation) operating in transmitter–receiver or pulse-echo mode. It is equipped with a 4 MHz, 128 elements, linear array transducer L14-5/38, with 0.3 mm element pitch, 0.02 kerf and 70% fractional bandwidth. Ultrasonix's platform enables full control of transmission and reception parameters for selected 128 consecutive channels activating the

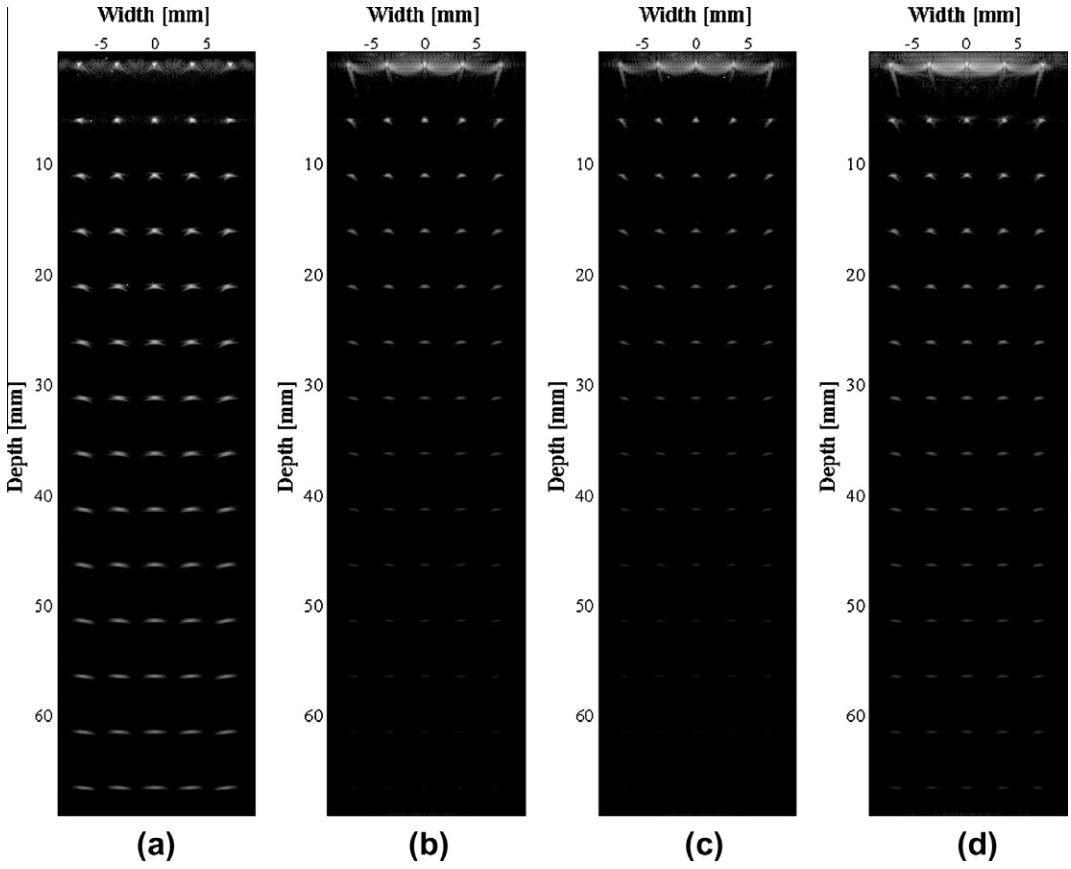

Fig. 5. Synthetic Aperture Algorithm (STA) image reconstructions (point reflectors) of the FIELD II simulated synthetic aperture data for point reflectors using 4 MHz, 64-element transducer array with 0.3 mm pitch and 0.02 mm kerf: (a) modified STA algorithm, this work, (b) Hamming apodized STA, (c) Blackman apodized STA, (d) conventional STA. All images are displayed over 50 dB dynamic range.

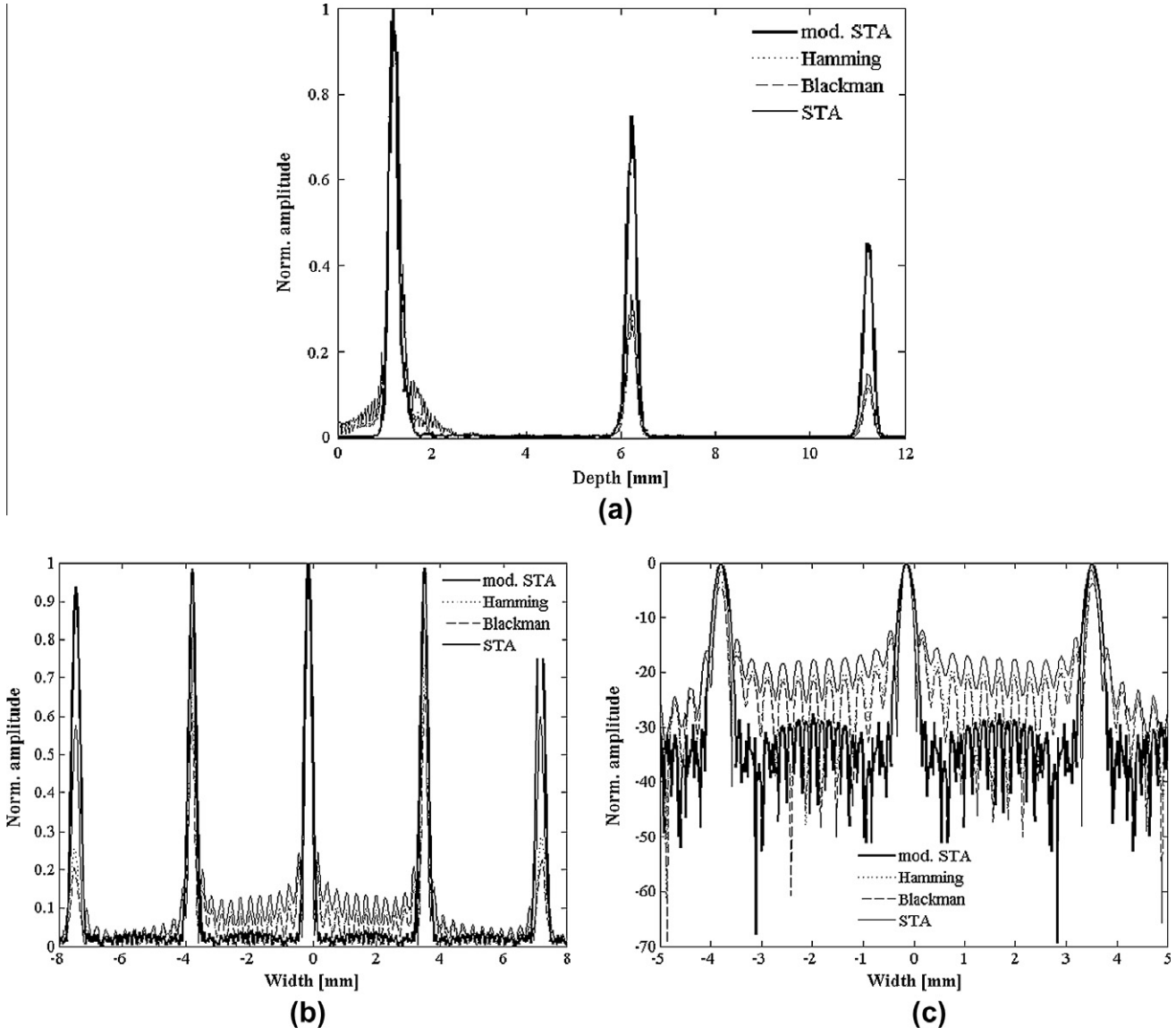

Fig. 6. Axial section of the central column: (a) lateral cross-section of the first row (axial depth of 1 mm) of point reflectors; thick solid lines – modified Synthetic Aperture Algorithm (STA), this work, thin solid lines – conventional STA, dotted lines – Hamming apodized STA, dashed lines – Blackman apodized STA: (b) normalized magnitude, (c) logarithmic scale.

individual elements of the array. In addition, full access to raw RF data allows their transfer to the PC (in digital form) for further processing in Matlab® in order to test the developed STA image reconstruction algorithm. After collecting the STA data the image reconstruction is processed off-line and – for any clinical diagnosis if needed – can be first made available once the signal processing is completed and the results of the scanning presented in cine-loop (virtual real-time) mode.

As already noted, in synthetic aperture imaging all scan lines (full image) are produced during each generation of the probing wave, whereas in conventional beamforming approach only a single line is created. Previous section discussion indicated that the amount of raw RF data needed for reconstruction of a single image in the STA algorithm is proportional to the product of the number of samples in a single RF image (D_{RF}) and the number of array elements squared (N^2). Thus, for the 128-element array, used in experiments described in the next section, and 10 cm penetration depth approximately 90e6 samples had to be stored (5500 samples per image line). This number of samples required approximately 0.18 GB of RAM. The overall initial estimate of the storage requirements was performed accounting for the Ultrasonix platform output data format, 2 bytes per sample. The image reconstruction (see numerical examples in Section 5, Fig. 10) was performed in Matlab® 7.11 on PC running Windows 7 × 64 with Athlon 64 X2 Dual Core 5600+, core speed 2.8 MHz. The estimated processing time (both for modified and conventional STA algorithm) was about 30 s. It should be noted that no attempts were made to optimize the Matlab code to shorten that (30 s) time.

5. Simulation and experimental results and discussion

In this section the results of the simulations performed with FIELD II [20,21] program for Matlab® are presented and compared with those obtained experimentally.

5.1. FIELD II simulations

To compare the lateral resolution and penetration depth of the conventional and the modified STA method FIELD II simulation was

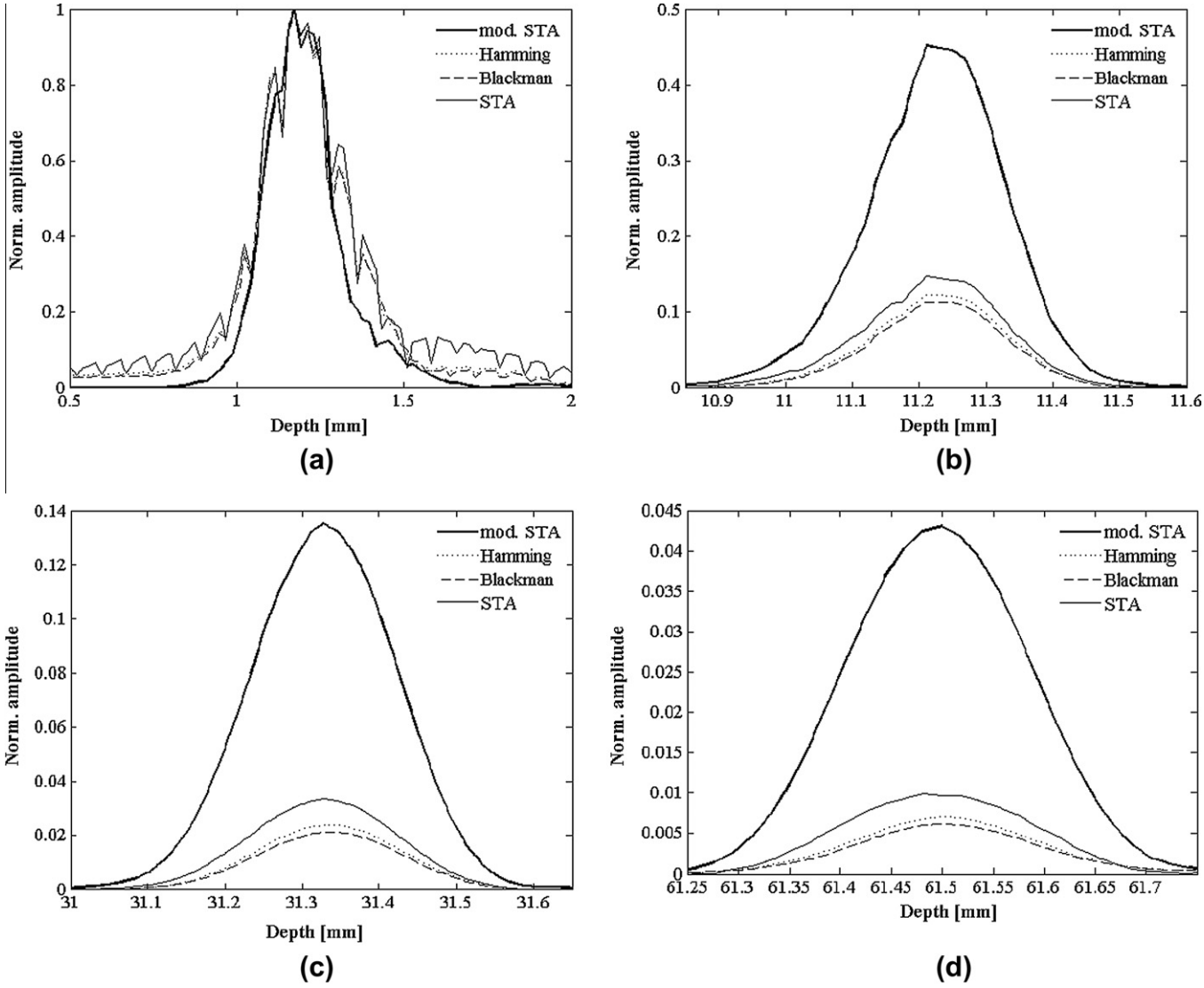

Fig. 7. Normalized axial section of the image line coinciding with the central column of point reflectors at different depths: (a) 1 mm, (b) 10 mm, (c) 30 mm, (d) 60 mm. Thick solid lines – modified Synthetic Aperture Algorithm (STA), this work, thin solid lines – conventional STA, dotted lines – Hamming apodized STA, dashed lines – Blackman apodized STA.

performed. More specifically, the echoes from point reflectors (detailed below) insonified by the 4 MHz, 64-element transducer array with the 0.3 mm pitch and 0.02 mm kerf were used as input data. Prior to presenting the results of the simulations it may be useful to briefly discuss the apparent discrepancy between the number of elements simulated (64) and those experimentally used (128). The primary reason for limiting the simulated array number of elements to 64 was the limitation due to the RAM memory used for Matlab code. Selecting 128 element transducer Field II simulation of point reflectors would require an excessively large matrix of data to be processed. In addition, the penetration depth would have to be at least doubled in order to illustrate the difference between the modified and conventional STA. The selection of 128 element transducer and 120 mm penetration depth results in the simulated data matrix of $16{,}384 \times 7000$, whereas in the case of 64 elements array and 70 mm depth the array is reduced to 4096×4000. In summary, to be able to display the lateral and axial cross-section as smooth as possible, the 64 elements array was intentionally chosen, but 1024 image lines (16 lines per pitch) were evaluated. In case of experimental data only 128 image lines (i.e. one line per pitch) were evaluated. Therefore, the number of image lines in 2D image was chosen to be 16 lines per pitch in the case of 64 element transducer for a total of 1024 image lines so a smooth shape curves shown in Figs. 6–8 could be obtained.

As shown in Fig. 5 the point reflectors were placed in 5 columns, each spaced 3.7 mm apart laterally (this corresponded to 12 transducer pitches). Such geometry, covering the whole imaging region, was considered to be appropriate for assessment of the image quality in the entire area. For convenience, the columns were centered with respect to the transducer middle point. In each column the axial distance between the reflectors was 5 mm. Such distance appears to be sufficient to demonstrate that the scattered echo signals amplitude decreases with increasing depth. The simulated 2D visualization of point reflectors is shown in Fig. 5 over a 50 dB dynamic range. Fig. 5a and d shows images obtained using the modified STA, discussed in this work, and the conventional one, respectively. For comparison, in Fig. 5b and c the images obtained using the STA algorithms with Hamming and Blackman apodization weights are shown. The FIELD simulated images of Fig. 5 support the notion that the modified STA algorithm is capable of enhancing the image quality, especially in the immediate vicinity (first raw) of the array surface. The blurring artefacts clearly visible

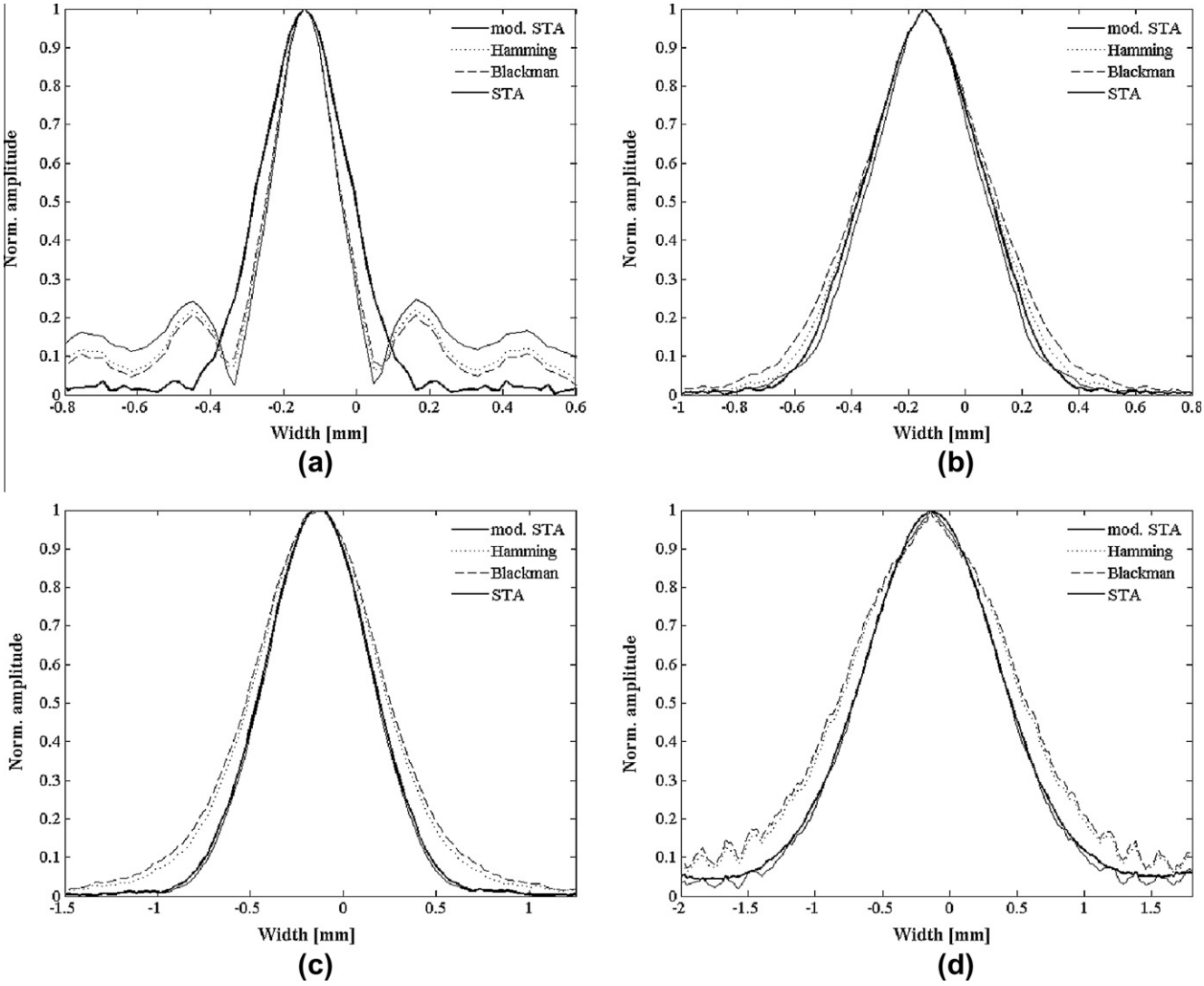

Fig. 8. Normalized lateral cross-sections corresponding to the scattered signal of the point reflectors placed in the central column at different depths: (a) 1 mm, (b) 10 mm, (c) 30 mm (d) 60 mm. Thick solid lines – modified Synthetic Aperture Algorithm (STA), this work, thin solid lines – conventional STA, dotted lines – Hamming apodized STA, dashed lines – Blackman apodized STA.

in Fig. 5b–d corresponding to Hamming apodized, Blackman apodized and conventional STA algorithm, respectively, in the vicinity of the first phantom row, are substantially reduced in Fig. 5a processed using the modified STA algorithm. Also, the penetration depth increases in the case of modified STA algorithm, see Fig. 5a, when compared with the conventional one, see Fig. 5b.

The image quality improvement is also visible in Fig. 6 where the axial section of the central column (only 3 first reflectors are shown for clarity) and the lateral cross-section of the first row of point reflectors are shown. As demonstrated in Fig. 6c the "noise"-like spatial variations of the scattered signal from the reflectors positioned near the transducer surface are substantially suppressed from approximately −17 dB obtained when applying conventional STA algorithm, to −29 dB corresponding to the level yielded by the modified STA. For comparison, the results obtained using the conventional STA algorithm with the smoothing Hamming and Blackman apodization weights are also shown. These indicate the "noise" reduction of approximately −21 dB as compared to conventional STA without the smoothing function or window.

Further analysis of Fig. 6 reveals that the modified STA method results in smoothing of the echo amplitudes corresponding to different (adjacent) point reflectors in the row in comparison both with the conventional STA algorithm and with those using Hamming and Blackman apodization weights. Specifically, the plots of Fig. 6a and b indicate that the ratio of scattered amplitudes corresponding to the last reflector in the row and the one situated in the center is equal to 0.94 for the modified STA and 0.57 for the conventional STA.

The already mentioned increase in the visualization depth (Fig. 5a and b) is further illustrated in Fig. 7 where a detailed view of the axial section (central column) showing the maxima of the scattered echo signals as a function of depth is presented. As shown in Fig. 7b–d in comparison with the conventional STA, the scattered echo amplitude obtained using the modified STA algorithm is {3.0, 4.1, 4.3} times larger at the depths of {10, 30, 60} mm, respectively. A comparison of the modified STA algorithm with the conventional one using Hamming and Blackman apodization weights indicates that the amplitudes are {3.7, 5.7, 6.2} and {4, 6.4, 7} times larger than the conventional STA method ones.

In Fig. 8 the results related to the lateral resolution are summarized. There, the lateral cross-sections corresponding to scattered echo signal of the point reflectors positioned in the central column are shown at different depths: 1, 10, 30 and 60 mm. As shown in

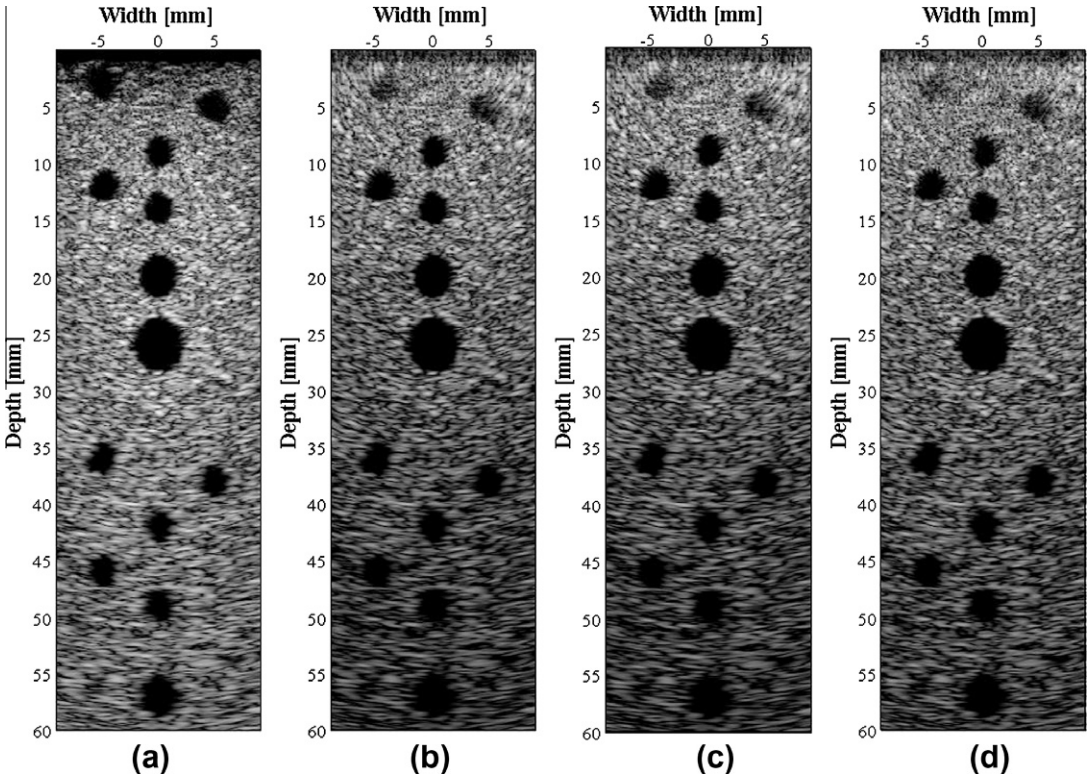

Fig. 9. STA image reconstruction of the FIELD II simulated synthetic aperture data for cyst phantom and 4 MHz 64-element transducer array with 0.3 mm pitch and 0.02 mm kerf (a) modified STA, this work, (b) Hamming apodized STA, (c) Blackman apodized STA, (d) conventional STA. All images are displayed over 50 dB dynamic range.

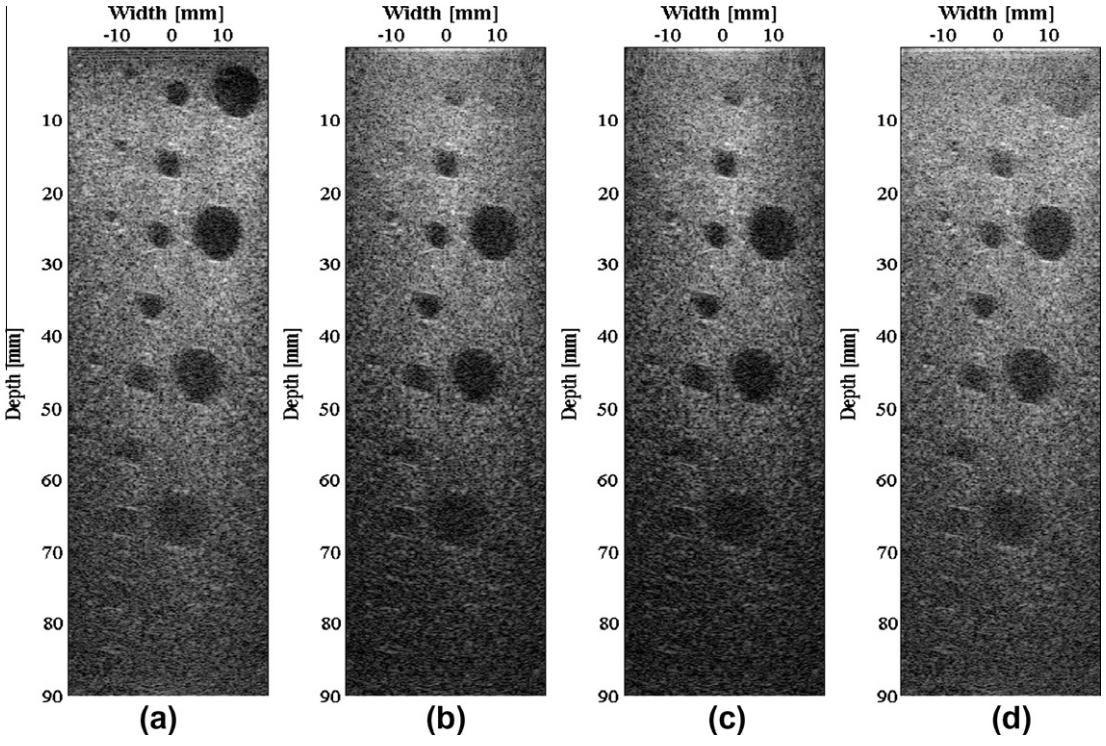

Fig. 10. STA image reconstruction of the measurement synthetic aperture data for cyst phantom (Dansk Fantom Service, model 571 [22]) and 4 MHz 128-element transducer array with 0.3 mm pitch and 0.02 mm kerf (a) modified STA, this work, (b) Hamming apodized STA, (c) Blackman apodized STA, (d) conventional STA. All images are displayed over 40 dB dynamic range.

Fig. 8a–d for modified STA algorithm the lateral resolution is slightly decreased in comparison with the one obtained by using the conventional STA. It is quantified here by the full width at half maximum (FWHM).

Accordingly, at the axial distances of 1, 10, 30 and 60 mm for the conventional STA the lateral resolution is 0.2012, 0.4425, 0.6476 and 1.1650 mm, respectively. The corresponding data for the modified STA are 0.2797, 0.4750, 0.6620 and 1.1778 mm and represent 28.1, 6.8, 2.2 and 1.1% decrease in the lateral resolution at the above identified depths. It is worth noting that the decrease in the lateral resolution decreases with increasing depth. Similar analysis performed for STA with Hamming and Blackman apodization weights (dashed and dotted lines in Fig. 8a–d) shows the respective lateral resolutions to be equal to 0.2043, 0.484, 0.7522 and 1.3525 mm (Hamming) and 0.2109, 0.5067, 0.7811 and 1.3917 mm (Blackman). Again, these values represent the respective decreases in lateral resolution of 1.5%, 8.6%, 14% and 13.9% (Hamming) and 4.6%, 12.3%, 17.1% and 16.3% (Blackman) as compared to the conventional STA processing. These data indicate that the modified STA algorithm at the depths below about 10 mm exhibits somewhat lower lateral resolution in comparison with that achieved with Hamming and Blackman apodizations. On the other hand, at the axial distances exceeding 10 mm, the lateral resolution of the modified STA algorithm exceeds those that were obtained using Hamming and Blackman windows.

In Fig. 9 the improvements in image contrast offered by the modified STA are demonstrated.

There, 2D visualization of the FIELD II simulated synthetic aperture data of a cyst phantom are shown The cyst phantom consisted of 300,000 point scatterers with equal reflectivity, randomly distributed (but with uniform distribution) over an area of 20×60 mm (lateral width $\times$ depth). Following the guidelines for speckle simulation [17,24] the number of scatterers was more than 10 per resolution cell. Thirteen cysts with zero reflectivity and different diameters were simulated. The diameters, which ranged from 3 mm to 5 mm were selected to be representative of those encountered in clinical practice as suggested in [25]. The 10 cysts having diameter of 3 mm were centered at the points identified in the following by the set of numbers corresponding to lateral width and depth, respectively: i.e. $(-5,2)$, $(5,4)$, $(0,8)$, $(-5,11)$, $(0,13)$, $(-5,35)$, $(5,37)$, $(0,41)$, $(-5,45)$ and $(0,48)$ mm. In addition, two cysts of 4 mm and one cyst of 5 mm in diameter were positioned at the points $(0,19)$, $(0,56)$ and $(0,25)$ mm, respectively. This positioning of the cysts was selected to facilitate the comparison of the penetration depths obtained with different algorithms. In addition, the cysts placed near the transducer aperture facilitated the demonstration of the noise reduction obtained with the modified STA.

In Fig. 9a and d the images obtained using the modified and conventional STA algorithms are shown. For comparison, in Fig. 9b and c the results of visualization by means of the STA algorithms with implemented Hamming and Blackman apodization weights are illustrated. As shown in Fig. 9a the modified STA algorithm provides better image quality of the cysts located in the vicinity of the transducer aperture in comparison with the conventional STA method, see Fig. 9d, as well as STA with Hamming and Blackman apodization, see Fig. 9b and c, respectively, and better image contrast with the increasing (penetration) depth.

5.2. Experimental results

In this section the performance of the modified STA algorithm is described. It was determined using the experimentally obtained synthetic aperture data of a cyst phantom (an extra large scan- and elevation-plane tissue mimicking phantom model 571 [25], Dansk Fantom Service). The measurements were done using the same (see Fig. 4) Sonix-TOUCH Research system (Ultrasonix Medical Corporation).

As anticipated (see Section 3), the results presented in Fig. 10, demonstrate that the modified STA algorithm (see Fig. 10a) provides a considerable improvement of the image quality in the immediate vicinity of the array's aperture (see Figs. 2 and 6c), where the large observation angles, (here corresponding to about 55–60°) occur. These large angles were quantified based on the careful analysis of the theoretical and experimental data and for the experimental conditions of this work were evaluated to be approximately 55–60°. At 55° the directivity pattern for an individual array element decreases by approximately 30% from its maximum level of 0 dB, i.e. to the level of negative 10 dB. This improvement is clearly visible when the image of Fig. 10a is compared with that of Fig. 10d, which shows the result obtained making use of the conventional algorithm. Similarly, the comparison of the images obtained the STA with Hamming- (Fig. 10b) and Blackman (Fig. 10c) windows with the image of Fig. 10a indicates the improved display structure close to the array's surface. Also, the results shown in Figs. 9 and 10, demonstrate that visually assessed image contrast of the cyst that are located at the axial distance exceeding 40 mm is also slightly improved (see Fig. 9). The phantom images of Fig. 10 indicate that in comparison to the conventional STA, the application of the synthetic aperture algorithm including Hamming, or Blackman apodization results in a slight improvement of images at the axial distance up to about 10 mm. However, this improvement is inferior to that obtained using the proposed modified STA approach.

6. Conclusions

The modified synthetic aperture algorithm for ultrasound imaging was developed and its performance was evaluated. In analogy to the time delays used in the realization of the conventional synthetic transmit aperture (STA) approach, the algorithm was implemented as a weighted sum of the appropriately delayed echo signals with weights calculated for each focal and for each transmit–receive pair. The weights were determined using the analytic expression for a far-field radiation pattern of a narrow strip (individual array element) transducer vibrating with uniform pressure amplitude distribution across its surface [12]. The appropriate synthetic aperture data were generated in Matlab® and subsequently input into FIELD II [20,21] for further processing. The FIELD II predicted improvements in the image quality and the penetration depth were then verified experimentally using cyst phantom. Specifically, using the modified STA a considerable (12 dB, see Fig. 6) improvement in the image quality in the "near field" region lying in the immediate vicinity of the transducer surface was observed. Also, the hazy blurring artefacts obtained using the conventional synthetic aperture algorithm were substantially (12 dB, see Fig. 6) suppressed due to the directivity weights applied in the modified STA. In addition, an increase in the visualization depth was demonstrated. In comparison with the conventional STA the simulated synthetic aperture data of point reflectors predicted the increase of the scattered amplitude at the depths of $\{10,30,60\}$ mm for the modified STA algorithm to be $\{3.0,4.1,4.3\}$ times, respectively. Concurrently, however, a slight degradation of the lateral resolution was observed; namely, at the depths of $\{1,10,30,60\}$ mm the modified STA algorithm provided the lateral resolution which was – correspondingly – $\{28.1,6.8,2.2,1.1\}$% lower than that achieved with the conventional STA. On the other hand this decrease in the lateral resolution decreased with increasing penetration depth.

It should be noted that the signal processing involved allowed off-line image reconstruction, only. In clinical practice that means that the delayed "real-time" image can be first made available once the signal processing is completed and the results of the scanning presented in a cine-loop mode. On the other hand, once the processing time is reduced so it can be performed in such a way that the image is updated at each launching of the probing wave, the

modified STA method would be well suited to be employed in clinical examinations, especially in the applications where the quality of the "near-field" image, that is the image in the immediate vicinity of the scanhead is of critical importance such as for instance in skin- and breast-examinations.

Acknowledgment

This work was supported by Grant No. NN518382137 from the Polish Ministry of Science and Higher Education.

References

[1] G.S. Kino, Acoustic Waves, Devices Imaging and Analog Signal Processing, Prentice Hall, Upper Saddle River, NJ, 1987.
[2] G. Montaldo, M. Tanter, J. Bercoff, N. Benech, M. Fink, Coherent plane-wave compounding for very high frame rate ultrasonography and transient elastography, IEEE Trans. Ultrason., Ferro elect., Freq. Cont. 56 (3) (2009) 489–506.
[3] J.J. Flaherty, K.R. Erikson, V.M. Lund, Synthetic aperture ultrasound imaging systems, Tech. rep., U.S. Patent 3 548 642, December 22, 1967.
[4] K. Nagai, A new synthetic-aperture focusing method for ultrasonic b-scan imaging by the Fourier-transform, IEEE Trans. Sonics Ultrason. 32 (4) (1985) 531–536.
[5] Y. Ozaki, H. Sumitani, T. Tomo da, M. Tanaka, A new system for real-time synthetic aperture ultrasonic imaging, IEEE Trans. Ultrason., Ferroelect., Freq. Cont. 35 (6) (1988) 828–838.
[6] C.R. Cooley, B.S. Robinson, Synthetic focus imaging using partial datasets, in: Proc. 1994 IEEE Ultrason. Symp. 1994, pp. 1539–1542.
[7] http://www.supersonicimagine.fr/.
[8] G.R. Lockwood, J.R. Talman, S.S. Brunke, Real-time 3-d ultrasound imaging using sparse synthetic aperture beamforming, IEEE Trans. Ultrason., Ferro elect., Freq. Cont. 45 (4) (1998) 980–988.
[9] J.S. Jeong, J.S. Hwang, M.H. Bae, T.K. Song, Effects and limitations of motion compensation in synthetic aperture techniques, in: Proc. 2000 IEEE Ultrason. Symp., 2000, pp. 1759–1762.
[10] J.A. Jensen, O. Holm, L.J. Jensen, H. Bendsen, S.I. Nikolov, B.G. Tomov, P. Munk, M. Hansen, K. Salomonsen, J. Hansen, K. Gormsen, H.M. Pedersen, K.L. Gammelmark, Ultrasound research scanner for real-time synthetic aperture data acquisition, IEEE Trans. Ultrason., Ferro elect., Freq. Cont. 52 (5) (2005) 881–891.
[11] J.A. Jensen, S.I. Nikolov, K.L. Gammelmark, M.H. Pedersen, Synthetic aperture ultrasound imaging, Ultrasonics 44 (2006) e5–e15.
[12] A.R. Selfridge, G.S. Kino, B.T. Khuriyakub, A theory for the radiation pattern of a narrow-strip acoustic transducer, Appl. Phys. Lett. 37 (1) (1980) 35–36.
[13] P.J. Thoen, Aperture apodization to reduce the o -axis intensity of the pulsed-mode directivity function of linear arrays, Ultrasonics 20 (5) (1982) 231–236.
[14] C.M.W. Daft, W.E. Engeler, Windowing of wide-band ultrasound transducers, in: Proc. 1996 IEEE Ultrason. Symp., 1996, pp. 1541–1544.
[15] K.E. Thomenius, Evolution of ultrasound beamformers, in: Proc. 1996 IEEE Ultrason. Symp., 1996, pp. 1615–1622.
[16] D.A. Guenther, W.F. Walker, Optimal apodization design for medical ultrasound using constrained least squares – part II: simulation results, IEEE Trans. Ultrason., Ferro elect., Freq. Cont. 54 (2) (2007) 343–358.
[17] J.F. Synnevg, A. Austeng, S. Holm, A low-complexity data-dependent beamformer, IEEE Trans. Ultrason., Ferro elect., Freq. Cont. 58 (2) (2011) 281–289.
[18] S. Repetto, A. Trucco, A stochastic approach for the apodization of very short arrays, Ultrasonics 42 (2004) 425–429.
[19] S.M. Sakhaei, A. Mahloojifar, H. Ghassemian, A transformation based method to design ultrasound array, Ultrasonics 49 (2) (2009) 179–184.
[20] J.A. Jensen, N.B. Svendsen, Calculation of pressure fields from arbitrarily shaped, apodized, and excited ultrasound transducers, IEEE Trans. Ultra-son., Ferro elect., Freq. Cont. 39 (2) (1992) 262–267.
[21] J.A. Jensen, Field: a program for simulating ultrasound systems, in: Proc. 10th Nordic-Baltic Conference on Biomedical Imaging published in Medical & Biological Engineering & Computing, vol. 34, no. 1, 1996, pp. 351–353.
[22] J.W. Goodman, Introduction to Fourier Optics, McGraw-Hill, Roberts and Company Publishers, 2005. p. 49.
[23] K. Michishita, K. Sakagami, M. Morimotgo, U.P. Svensson, Sound radiation from an unbaffled elastic plate strip of infinite length, Appl. Acoust. 61 (2000) 45–63.
[24] R.F. Wagner, S.W. Smith, J.M. Sandrik, H. Lopez, Statistics of speckle in ultrasound b-scans, IEEE Trans. Sonics Ultrason. 30 (3) (1983) 156–163.
[25] http://fantom.dk/571.htm.